


EXPRESS LETTER

Open Access



The 2018 Hokkaido Eastern Iburi earthquake ($M_{JMA} = 6.7$) was triggered by a strike-slip faulting in a stepover segment: insights from the aftershock distribution and the focal mechanism solution of the main shock

Kei Katsumata^{1*} , Masayoshi Ichiyanagi¹, Mako Ohzono¹, Hiroshi Aoyama¹, Ryo Tanaka¹, Masamitsu Takada¹, Teruhiro Yamaguchi¹, Kazumi Okada¹, Hiroaki Takahashi¹, Shin'ichi Sakai², Satoshi Matsumoto³, Tomomi Okada⁴, Toru Matsuzawa⁴, Shuichiro Hirano⁵, Toshiko Terakawa⁶, Shinichiro Horikawa⁶, Masahiro Kosuga⁷, Hiroshi Katao⁸, Yoshihisa Iio⁸, Airi Nagaoka⁸, Noriko Tsumura⁹, Tomotake Ueno¹⁰ and the Group for the Aftershock Observations of the 2018 Hokkaido Eastern Iburi Earthquake

Abstract

The Hokkaido Eastern Iburi earthquake ($M_{JMA} = 6.7$) occurred on September 6, 2018, in the Hokkaido corner region where the Kurile and northeastern Japan island arcs meet. We relocated aftershocks of this intraplate earthquake immediately after the main shock by using data from a permanent local seismic network and found that aftershock depths were concentrated from 20 to 40 km, which is extraordinarily deep compared with other shallow intraplate earthquakes in the inland area of Honshu and Kyushu, Japan. Further, we found that the aftershock area consists of three segments. The first segment is located in the northern part of the aftershock area, the second segment lies in the southern part, and the third segment forms a stepover between the other two segments. The hypocenter of the main shock, from which the rupture initiated, is located on the stepover segment. The centroid moment tensor solution for the main shock indicates a reverse faulting, whereas the focal mechanism solution determined by using the first-motion polarity of the *P* wave indicates strike-slip faulting. To explain this discrepancy qualitatively, we present a model in which the rupture started as a small strike-slip fault in the stepover segment of the aftershock area, followed by two large reverse faulting ruptures in the northern and southern segments.

Keywords: The Hokkaido Eastern Iburi earthquake, Strike-slip fault, Reverse fault, Aftershock distribution, Focal mechanism solution, Local seismic network, Stepover segment

Introduction

The Hokkaido Eastern Iburi earthquake occurred on September 6, 2018, and the parameters of the hypocenter given by the Japan Meteorological Agency (JMA) are as follows: origin time = 03:07:59.3 JST,

epicenter = (42.691°N, 142.007°E), depth = 37.0 km, and $M_{JMA} = 6.7$. This earthquake is located in the Hokkaido corner region, where the northern Japan island arcs connect to the Kurile Islands. The Pacific plate subducts beneath Hokkaido Island on the North American or the Okhotsk Sea Plate in this region (e.g., Takahashi et al. 1999; Katsumata et al. 2002). In addition, the Kurile island arc is moving toward the southwest and colliding with the northeastern Japan arc (e.g., Kimura 1996). This region is called the arc–arc-type Hidaka

*Correspondence: kkatsu@sci.hokudai.ac.jp

¹ Faculty of Science, Institute of Seismology and Volcanology, Hokkaido University, Sapporo, Japan

Full list of author information is available at the end of the article

collision zone (HCZ). The depth to the upper surface of the subducting Pacific plate is approximately 100 km around the focal area (Katsumata et al. 2003); therefore, this earthquake obviously occurred in the North American plate or the Okhotsk Sea plate, i.e., this earthquake was a shallow intraplate earthquake in the inland area of Japan.

The first purpose of this study is to re-evaluate the depth and distribution of the main shock and aftershocks accurately. The hypocenters of main shocks are usually shallower than 20 km for shallow intraplate earthquakes in the inland area of Japan (Omuralieva et al. 2012), whereas the depth of this sequence was obviously deeper than 20 km according to the preliminary report from the JMA. Therefore, we relocated the hypocenters of the main shock and aftershocks in this study by considering a local complex velocity structure of the crust.

The second purpose of this study is to investigate the reason for the mismatch between the centroid moment tensor (CMT) solution and the focal mechanism solution determined by using the first-motion polarities of P waves at individual stations. The CMT solutions of the main shock were reported by four groups: JMA (2018a), the National Research Institute for Earth Science and Disaster Resilience (NIED 2018a), the United States Geological Survey (USGS 2018), and the Global CMT project (Dziewonski et al. 1981; Ekström et al. 2012). All CMT solutions of this earthquake are consistent in showing that the earthquake resulted mainly from reverse faulting. However, the focal mechanism of this earthquake was mainly strike-slip faulting (JMA 2018b; NIED 2018b). We estimated the focal mechanism solution by adding data from seismic stations in the focal area and investigated a model to explain qualitatively the discrepancy between the CMT solutions and the focal mechanisms by referring to the relocated aftershock distribution.

Data

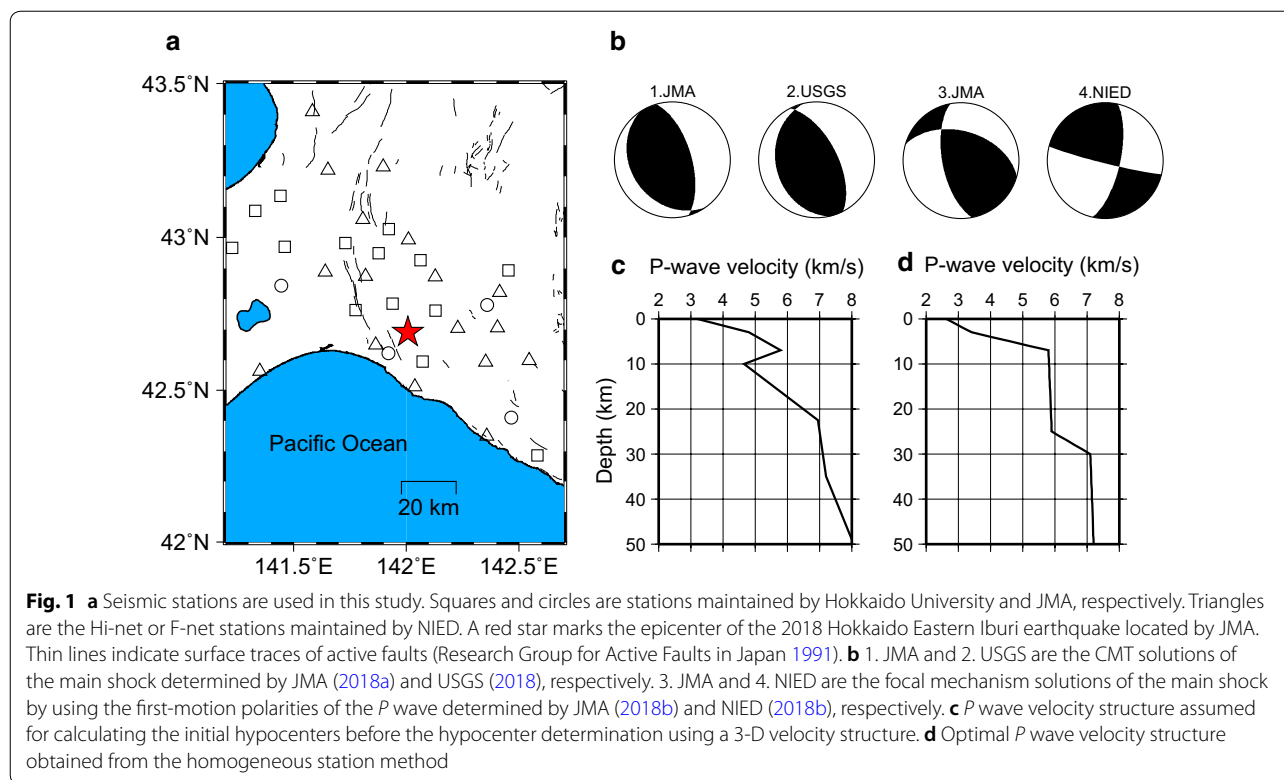
We used the arrival times of P and S waves from 35 permanent seismic stations maintained by Hokkaido University, JMA, and NIED (Fig. 1). Each station consists of a short-period seismograph with three components on the ground surface or in a vertical borehole. All waveform data are telemetered continuously in real time, and preliminary hypocenters are determined automatically. In total, 459 earthquakes were detected and located for ~ 2 days between 2018-09-06 03:00 and 2018-09-07 23:59, and we used the arrival times from these earthquakes in the following analyses. All waveform data were examined carefully by visual inspection, and all arrival times were read manually by a well-trained person. The

accuracies for most P and S arrival times are considered to be 0.05–0.1 s and 0.1–0.2 s, respectively. An electrical power loss occurred during this period, and the waveform data were not recorded for several hours at some stations. We deployed 25 temporary seismic stations in the focal area immediately after the main shock and observed aftershocks for approximately 2 months. Although we successfully recorded many earthquakes, we used no data from the temporary seismic stations in this study.

Analyses

To relocate hypocenters, we first determine hypocenters of earthquakes with an assumption of a 1-D velocity structure using the hypomh algorithm (Hirata and Matsu'ura 1987). We then used the hypocenters as the initial locations of earthquakes and carried out relative hypocenter relocation using double-difference tomography (tomoDD) (Zhang and Thurber 2003) with a fixed 3-D velocity structure. The initial locations of hypocenters were calculated with an assumption of a 1-D structure for the velocity of the P wave (V_p) based on Iwasaki et al. (2004) as shown in Fig. 1c: 3.2 km/s at 0.0 km depth, 4.8 km/s at 3.0 km, 5.78 km/s at 7.0 km, 4.65 km/s at 10.0 km, 6.95 km/s at 22.5 km, 7.2 km/s at 35.0 km, and 8.06 km/s at 50.0 km. The velocity of the S wave (V_s) was calculated at each depth as $V_p/1.73$ with the assumption that the V_p/V_s ratio is 1.73. Recently several authors presented a 3-D tomographic model of V_p and V_s in this region (Katsumata et al. 2006; Yoshida et al. 2007; Kita et al. 2012; Shiina et al. 2018); thus, we assumed a 3-D velocity structure as shown in Additional file 1. The study area was divided into grids every 10 km in both the longitude and latitude directions on each plane at depths of 0, 5, 10, 22.5, 35, and 50 km. Values of V_p and the V_p/V_s ratio at depths shallower than 10 km were based on Yoshida et al. (2007), and those at depths equal to and deeper than 10 km were based on Shiina et al. (2018).

To support the results obtained by the method described above, we determined the hypocenters by using a homogeneous station method. Seven seismic stations were selected among the 35 stations, and their epicentral distances from the main shock ranged from 14 to 38 km. Seventy aftershocks were relocated for the 4 h immediately after the main shock between 2018-09-06 03:15 and 07:18. The arrival times of both P and S waves were picked at all seven stations for all 70 aftershocks; thus, hypocenters have no variations due to differences in the combination of seismic stations. We used the hypomh program (Hirata and Matsu'ura 1987) to determine hypocenters, and the 1-D V_p structure was assumed to be as follows: 2.6 km/s at a depth



of 0 km, 3.4 km/s at a depth of 3 km, and 5.8 km/s at a depth of 7 km. These values are based on Iwasaki et al. (2004). The V_p structure at depths deeper than 7 km was assumed to be as follows: V_1 km/s at a depth of $(7 + H)$ km, V_2 km/s at a depth of $(7 + H) + 5$ km, and 9.0 km/s at a depth of $(7 + H) + 5 + 370$ km. The four parameters, V_1 , V_2 , H , and the V_p/V_s ratio, were determined using a grid search technique. V_1 , V_2 , H , and the V_p/V_s ratio ranged from 5.9 to 7.9 km/s with every 0.1 km/s, from $V_1 + 0.1$ to 8.5 km/s with every 0.1 km/s, from 1 to 50 km with every 1 km, and from 1.60 to 1.80 with every 0.01, respectively. The optimal solution for the four parameters was determined under the condition that the residual of the 70 aftershocks reaches a minimum.

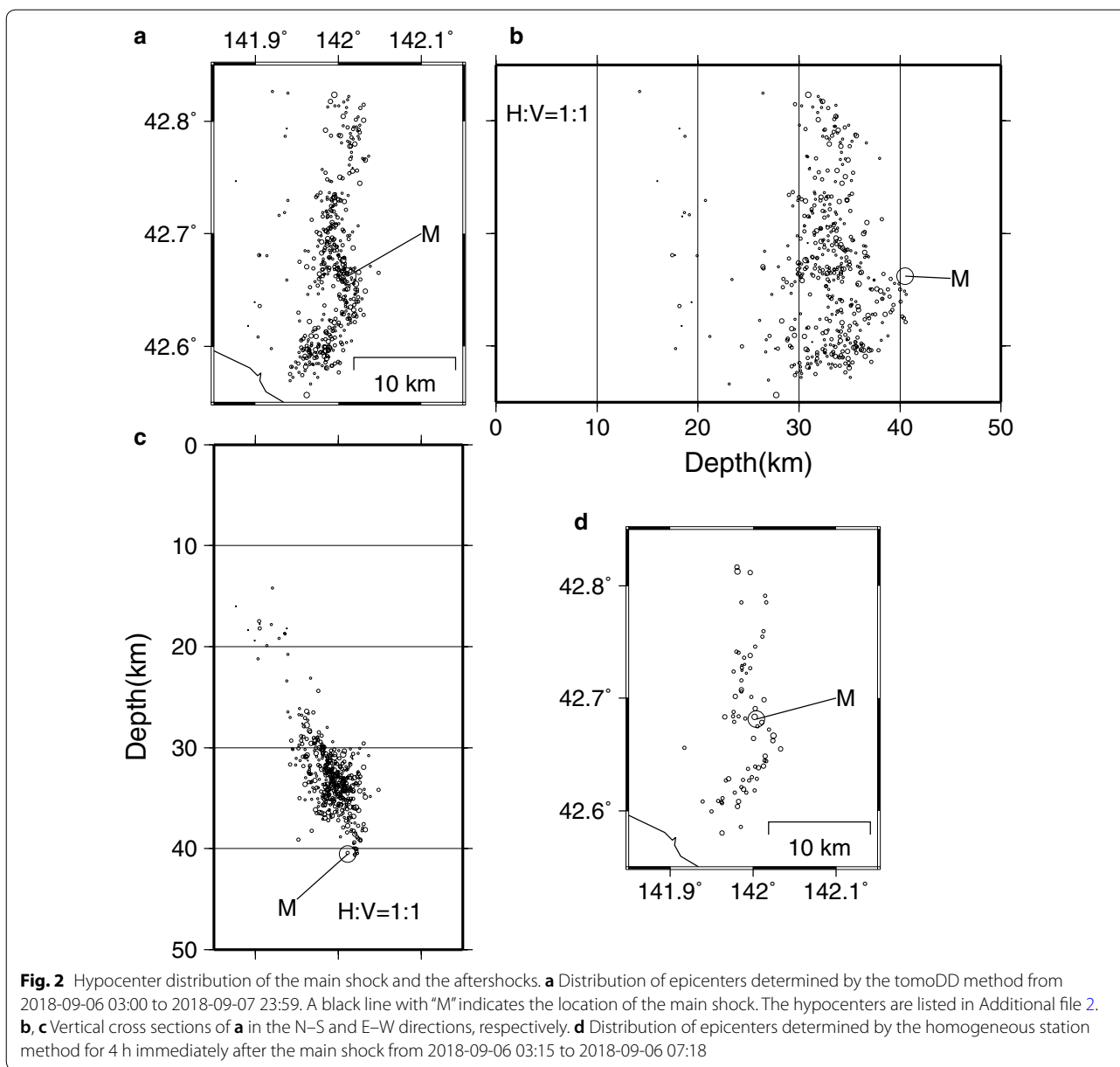
To determine the focal mechanism solution of the main shock, we used the HASH method (Hardebeck and Shearer 2002), which is a grid search program using the first-motion polarity of the *P* wave. *P* wave first-motion polarities were read manually by careful inspection at 53 seismic stations with epicentral distances from 9 to 114 km. No amplitude data were used.

Results

In total, 459 earthquakes were located for ~2 days between 2018-09-06 03:00 and 2018-09-07 23:59 (Fig. 2 and Additional file 2). We located the epicenter of the

main shock at (42.662°N, 142.011°E), and the depth was 40.5 km. We found that the aftershock area extended 25 km horizontally, approximately in the N–S direction, and that 95% of the hypocenters were distributed at depths from 20 to 40 km. The location errors were approximately 0.2 km in both the horizontal and vertical directions for the relocated main shock and aftershocks. These small errors indicated that the reading error depending on the ground noise level was very small and that the station coverage was very good. Zero, 14, 50, 387, and 8 hypocenters were located shallower than 10 km, 10 to 20 km, 20 to 30 km, 30 to 40 km, and 40 to 50 km, respectively. Therefore, the aftershocks of the 2018 Hokkaido Eastern Iburi earthquake occurred at the obviously greater depths than other intraplate earthquakes in the inland area of Honshu and Kyushu, Japan.

We also found that the aftershock area consists of three segments: the northern, the southern, and the stepover segments. Taking location errors into account, possible fault zones are shown in each vertical cross section in Fig. 3. The northern segment extends horizontally 15 km in the N–S direction and dips ~60° to the east. The southern segment extends horizontally 10 km in the NNE–SSW direction and dips ~65° to the ESE. The near-N–S horizontal trends and the dip angles of these two segments are consistent with one of the nodal planes of the CMT solutions, indicating that the main shock was



mainly due to reverse thrust faulting. Both the horizontal lengths and the dip angles are almost the same for the northern and southern segments, whereas the horizontal direction of the southern segment is rotated slightly clockwise relative to the northern segment. Moreover, a clear horizontal offset or stepover of ~ 5 km is observed between the two segments. This stepover segment extends horizontally 5 km in the WNW-ESE direction and seems to connect the southern and northern segments. The hypocenter of the main shock, i.e., the initiation point of the rupture, is located in the stepover segment.

In the case of the homogeneous station method, the optimal solutions for the four parameters are as follows (Fig. 1d): $V_1 = 5.9$ km/s, $V_2 = 7.1$ km/s, $H = 18$ km, and $V_p/V_s = 1.70$. By using the optimal 1-D velocity structure, we located the epicenter of the main shock at (42.681°N, 142.004°E), and the depth was 34.3 km. The spatial patterns described above were also obtained in the homogeneous station method analysis, as shown in Fig. 2. The different analyses presented similar results. Therefore, the two noteworthy spatial patterns obtained in this study, i.e., (1) the deep distribution of aftershocks and (2) the aftershock area consisting of three segments, seemed to be reliable.

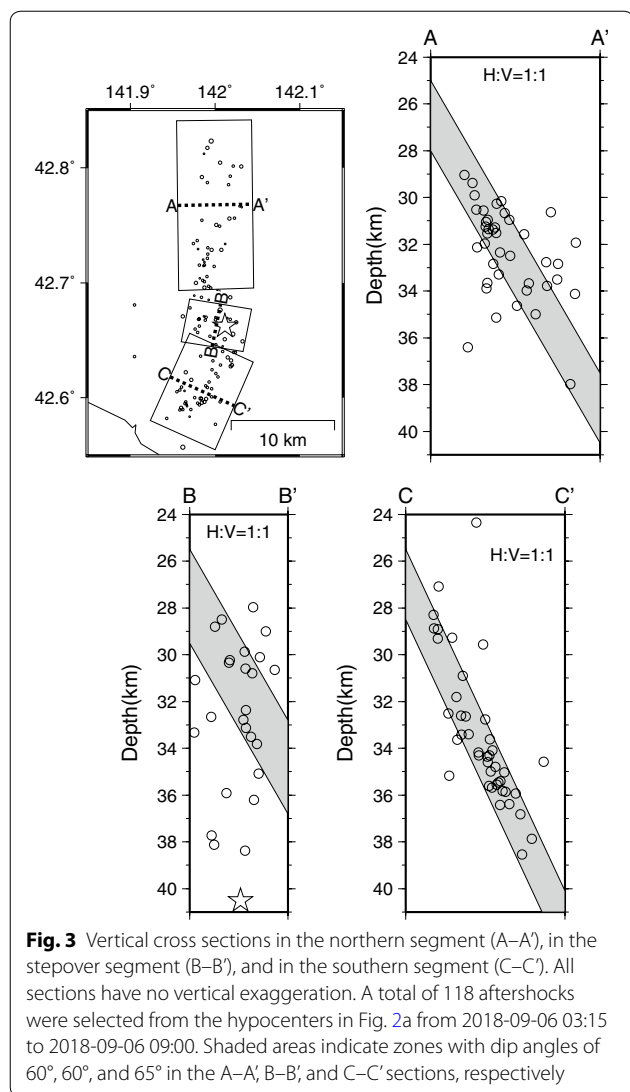


Fig. 3 Vertical cross sections in the northern segment (A–A’), in the stepover segment (B–B’), and in the southern segment (C–C’). All sections have no vertical exaggeration. A total of 118 aftershocks were selected from the hypocenters in Fig. 2a from 2018-09-06 03:15 to 2018-09-06 09:00. Shaded areas indicate zones with dip angles of 60°, 60°, and 65° in the A–A’, B–B’, and C–C’ sections, respectively

We obtained the focal mechanism solution of the main shock: nodal plane 1 (strike, dip, rake) = (177°, 73°, 143°) and nodal plane 2 (279°, 54°, 20°) (Fig. 4). As the station coverage was good and the misfit was small, the quality of solution was estimated to be A (good) by the HASH program. The solution in this study indicated strike-slip faulting with a small component of reverse faulting and did not match the CMT solutions. On the other hand, the strike of nodal plane 2 was estimated in the WNW-ESE direction, which was consistent with the direction of the aftershock distribution in the stepover segment.

Discussion

Extraordinarily deep aftershock distribution

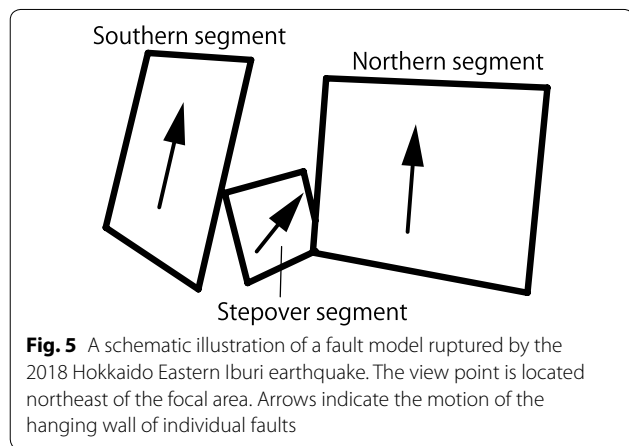
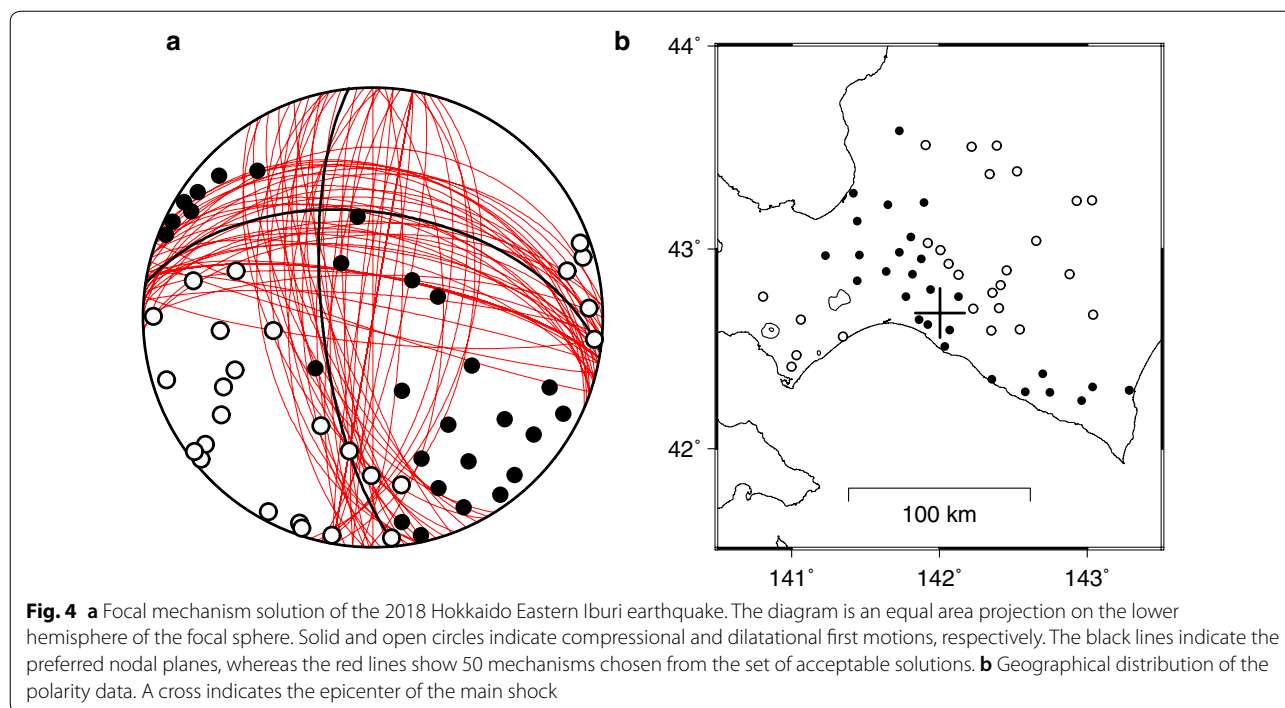
In this study, we relocated the main shock and the aftershocks of the 2018 Hokkaido Eastern Iburi earthquake

and found that almost all earthquakes were concentrated at depths from 20 to 40 km. This range is extraordinarily deeper than other intraplate earthquakes in the inland area of Honshu and Kyushu, Japan. Table S1 in Additional file 3 shows that in the case of the 1995 Hyogo-ken–Nanbu earthquake (M_{JMA} 7.2), the depth range of the aftershock area is from 0 to 20 km (Hirata et al. 1996); the 2000 Western Tottori (M_{JMA} 7.3), 2–13 km (Shibutani et al. 2005); the 2004 mid-Niigata (M_{JMA} 6.8), 2–13 km (Okada et al. 2005); the 2005 West Off Fukuoka (M_{JMA} 7.0), 2–16 km (Shimizu et al. 2006); the 2007 Chuetsu-oki (M_{JMA} 6.8), 5–22 km (Nakahigashi et al. 2012); the 2007 Noto Hanto (M_{JMA} 6.9), 1–13 km (Sakai et al. 2008); the 2008 Iwate-Miyagi Nairiku (M_{JMA} 7.2), 2–8 km (Okada et al. 2012); the 2011 Iwaki (M_{JMA} 7.0), 2–15 km (Kato et al. 2013); the 2016 Kumamoto (M_{JMA} 7.3), 2–18 km (Shito et al. 2017); and the 2016 Tottori (M_{JMA} 6.6), 5–15 km (Ross et al. 2018). On the other hand, the aftershock area is deep in and around the HCZ, Hokkaido. For example, in the cases of the 1970 M_{JMA} = 6.7 Hidaka earthquake and the 1982 M_{JMA} = 7.1 Urakawa-oki earthquake, the aftershocks were located at depths from 20 to 30 km and from 18 to 35 km, respectively (Moriya 1972; Moriya et al. 1983). The 2018 Hokkaido Eastern Iburi earthquake is also located in the HCZ and its deep distribution of aftershocks is very similar to those of previous earthquakes in this region.

The hypocenter of the 2018 earthquake is located near the bottom of the aftershock area. This fact is consistent with a model in which the stress accumulates on a seismic fault in the upper crust due to a weak zone in the lower crust (Iio et al. 2002). The *P* and *S* wave velocities, the resistivity, and the pore pressure in and around the aftershock area provide clues for further discussion.

A model of the fault ruptures during the main shock

Here, we first summarize the results: (1) the hypocenter of the main shock was located in the stepover segment in the central part of the aftershock area and (2) the focal mechanism solution of the main shock is consistent with the aftershock distribution in the stepover segment. Based on these results, we present a model in which the fault rupture during the main shock started at the stepover segment in a small area, possibly $5 \times 5 \text{ km}^2$ and $M \sim 5$, with left-lateral strike-slip faulting, and immediately afterward, large ruptures, possibly with fault areas of $10 \times 10 \text{ km}^2$ and $M \sim 6.4$ each, were triggered in the northern and southern segments with reverse faulting (Fig. 5). Nodal plane 2 of the focal mechanism obtained in this study probably corresponds to the first strike-slip faulting, which dips toward the NNE; thus, the hanging wall of this fault plane moved westward and upward.



Qualitatively, these motions possibly promoted reverse faulting in the northern and southern segments. To test the fault model, the Coulomb failure stress change (ΔCFS) in and around the focal area was calculated (see Additional file 4). In the case of the 2007 Noto Hanto earthquake, Sakai et al. (2008) also proposed a model in which small strike-slip faulting occurred first, and 0.6 s later, the main rupture with reverse faulting was triggered by the small strike-slip faulting. The model presented in this study should be supported by other data and analyses, including far-field body waves, near-field strong motion records, global

navigation satellite system (GNSS), and interferometric synthetic aperture radar (InSAR).

The rupture process including a stepover segment is well known in the case of strike-slip faulting, e.g., the 1992 M_w 7.3 Landers earthquake (Sieh et al. 1993) and the 2016 M_w 7.8 Kaikoura, New Zealand earthquake (Hamling et al. 2017). Many numerical simulations and theoretical studies on the physical mechanism of rupture propagation consider a stepover segment between strike-slip faults (e.g., Bai and Ampuero 2017). However, little is known about the rupture process with a stepover segment in the case of reverse thrust faulting. In this sense, the 2018 Hokkaido Eastern Iburi earthquake is an unusual earthquake.

Conclusions

We relocated hypocenters of the main shock and aftershocks immediately after the 2018 Hokkaido Eastern Iburi earthquake ($M_{JMA}=6.7$) by using two different methods: the hypoDD method with an assumed 3-D velocity structure and a homogeneous station method. As a result, we found that the main shock was located obviously deeper than 30 km, and almost all aftershocks were located at depths between 20 and 40 km. These depths are extraordinarily deeper than those for other intraplate earthquakes in the inland area of Japan. The CMT solution of the main shock is inconsistent with the focal mechanism solution determined by the first-motion polarities of the P wave. This discrepancy is probably

explained by the model proposed in this study in which the rupture started as a small left-lateral strike-slip fault in the stepover segment, and afterward, two large reverse faults were triggered in the northern and southern segments.

Additional files

Additional file 1. 3D P wave velocity structure.

Additional file 2. List of hypocenters in Fig. 2a, b, and c.

Additional file 3: Table S1. Depth range of aftershock area.

Additional file 4. A calculation of the Coulomb stress change.

Acknowledgements

We thank Takuji Yamada and an anonymous reviewer for valuable comments. We used waveform data from seismic stations maintained by JMA, and we also used waveform data from Hi-net (High-Sensitivity Seismograph Network of Japan) and F-net (Broadband Seismograph Network) maintained by NIED. We used observation equipment at some seismic stations supported by the Earthquake Research Institute Joint Usage/Research Program. GMT-SYSTEM (Wessel and Smith 1991) was used for mapping data. MICAP-G (Naito and Yoshikawa 1999) was used to calculate changes in the Coulomb failure stress.

A list of individual members of the Group for the Aftershock Observations of the 2018 Hokkaido Eastern Ibari Earthquake follows: Kei Katsumata¹, Masayoshi Ichianagi¹, Mako Ohzono¹, Hiroshi Aoyama¹, Ryo Tanaka¹, Masamitsu Takada¹, Teruhiro Yamaguchi¹, Kazumi Okada¹, Hiroaki Takahashi¹, Shin'ichi Sakai², Koji Miyakawa², Shin'ichi Tanaka², Miwako Ando², Satoshi Matsumoto³, Tomomi Okada⁴, Toru Matsuzawa⁴, Naoki Uchida⁴, Ryosuke Azuma⁴, Ryota Takagi⁴, Keisuke Yoshida⁴, Takashi Nakayama⁴, Satoshi Hirahara⁴, Toshiko Terakawa⁵, Yoshiko Yamanaka⁵, Yuta Maeda⁵, Shinichiro Horikawa⁵, Shuichiro Hirano⁶, Hiroki Miyamachi⁶, Hiroshi Yakiwara⁶, Masahiro Kosuga⁷, Takuto Maeda⁷, Hiroshi Katao⁸, Yoshihisa Iio⁸, Airi Nagaoka⁸, Noriko Tsumura⁹, Masahiro Shimazaki⁹, Tomotake Ueno¹⁰, and Youichi Asano¹⁰, where ¹ Hokkaido University, ² University of Tokyo, ³ Kyushu University, ⁴ Tohoku University, ⁵ Nagoya University, ⁶ Kagoshima University, ⁷ Hirosaki University, ⁸ Kyoto University, ⁹ Chiba University, and ¹⁰ National Research Institute for Earth Science and Disaster Resilience.

Authors' contributions

MI read all arrival times of P and S waves and determined hypocenters using the tomoDD method. KK performed the homogeneous station method analysis, the HASH analysis and was a major contributor in writing the manuscript. MO, HA, RT, MT, TY, KO, and HT are the technical staff members who maintain the seismic stations of Hokkaido University. SS, SM, TO, TM, SH, TT, SH, MK, HK, YI, AN, NT, TU, and members of the Group for the Aftershock Observations are the assistant staff to maintain the seismic stations. All authors read and approved the final manuscript.

Funding

This study was partly supported by the Ministry of Education, Culture, Sports, Science and Technology (MEXT) of Japan, under its Earthquake and Volcano Hazards Observation and Research Program. This study was also partly supported by MEXT KAKENHI Grant JP18K119952.

Availability of data and materials

The datasets used and/or analyzed during the current study are available from the corresponding author on reasonable request.

Competing interests

The authors declare that they have no competing interests.

Author details

¹ Faculty of Science, Institute of Seismology and Volcanology, Hokkaido University, Sapporo, Japan. ² Earthquake Research Institute, University of Tokyo, Tokyo, Japan. ³ Institute of Seismology and Volcanology, Kyushu University, Fukuoka, Japan. ⁴ Research Center for Prediction of Earthquakes and Volcanic Eruptions, Tohoku University, Sendai, Japan. ⁵ Nansai-Toko Observatory for Earthquakes and Volcanoes, Graduate School of Science and Engineering, Kagoshima University, Kagoshima, Japan. ⁶ Earthquake and Volcano Research Center, Graduate School of Environmental Studies, Nagoya University, Nagoya, Japan. ⁷ Earthquake and Volcano Observatory, Hirosaki University, Hirosaki, Japan. ⁸ Disaster Prevention Research Institute, Kyoto University, Kyoto, Japan. ⁹ Department of Earth Science, Faculty of Science, Chiba University, Chiba, Japan. ¹⁰ National Research Institute for Earth Science and Disaster Resilience, Tsukuba, Japan.

Received: 24 December 2018 Accepted: 23 April 2019

Published online: 20 May 2019

References

- Bai K, Ampuero J-P (2017) Effect of seismogenic depth and background stress on physical limits of earthquake rupture across fault step overs. *J Geophys Res Solid Earth* 122:10280–10298. <https://doi.org/10.1002/2017JB014848>
- Dziewonski AM, Chou T-A, Woodhouse JH (1981) Determination of earthquake source parameters from waveform data for studies of global and regional seismicity. *J Geophys Res* 86:2825–2852. <https://doi.org/10.1029/JB086iB04p02825>
- Ekström G, Nettles M, Dziewonski AM (2012) The global CMT project 2004–2010: centroid-moment tensors for 13,017 earthquakes. *Phys Earth Planet Inter* 200–201:1–9. <https://doi.org/10.1016/j.pepi.2012.04.002>
- Hamling IJ et al (2017) Complex multifault rupture during the 2016 M_w 7.8 Kaikōura earthquake, New Zealand. *Science* 356:eaam7194. <https://doi.org/10.1126/science.aam7194>
- Hardebeck JL, Shearer PM (2002) A new method for determining first-motion focal mechanisms. *Bull Seism Soc Am* 92:2264–2276. <https://doi.org/10.1785/0120010200>
- Hirata N, Matsu'ura M (1987) Maximum-likelihood estimation of hypocenter with origin time eliminated using nonlinear inversion technique. *Phys Earth Planet Inter* 47:50–61. [https://doi.org/10.1016/0031-9201\(87\)90066-5](https://doi.org/10.1016/0031-9201(87)90066-5)
- Hirata N et al (1996) Urgent joint observation of aftershocks of the Hyogo-ken Nanbu earthquake. *J Phys Earth* 44:317–328. <https://doi.org/10.4294/jpe1952.44.317>
- Iio Y, Sagiya T, Kobayashi Y, Shiozaki I (2002) Water-weakened lower crust and its role in the concentrated deformation in the Japanese Islands. *Earth Planet Sci Lett* 203:245–253. [https://doi.org/10.1016/S0012-821X\(02\)00879-8](https://doi.org/10.1016/S0012-821X(02)00879-8)
- Iwasaki T et al (2004) Upper and middle crustal deformation of an arc-arc collision across Hokkaido, Japan, inferred from seismic refraction/wide-angle reflection experiments. *Tectonophysics* 388:59–73. <https://doi.org/10.1016/j.tecto.2004.03.025>
- JMA (2018a) The CMT solutions. <https://www.data.jma.go.jp/svd/eqev/data/mech/cmt/fig/cmt20180906030759.html>. Accessed 29 Nov 2018
- JMA (2018b) Focal mechanism solutions by using first motion polarities. <https://www.data.jma.go.jp/svd/eqev/data/mech/ini/fig/mc20180906030759.html>. Accessed 29 Nov 2018
- Kato A et al (2013) Imaging the source regions of normal faulting sequences induced by the 2011 M9.0 Tohoku-Oki earthquake. *Geophys Res Lett* 40:273–278. <https://doi.org/10.1002/grl.50104>
- Katsumata K et al (2002) Distribution of hypocenters and focal mechanisms in and around the Hidaka arc-arc collision zone revealed by a dense temporary seismic network. *Bull Earthq Res Inst Univ Tokyo* 77:199–223
- Katsumata K, Wada N, Kasahara M (2003) Newly imaged shape of the deep seismic zone within the subducting Pacific plate beneath the Hokkaido corner, Japan-Kurile arc-arc junction. *J Geophys Res* 108(B12):2565. <https://doi.org/10.1029/2002JB002175>

- Katsumata K, Wada N, Kasahara M (2006) Three-dimensional P and S wave velocity structures beneath the Hokkaido corner, Japan-Kurile arc-arc junction. *Earth Planets Space* 58:e37–e40. <https://doi.org/10.1186/BF03352595>
- Kimura G (1996) Collision orogeny at arc-arc junctions in the Japanese Islands. *Island Arc* 5:262–275. <https://doi.org/10.1111/j.1440-1738.1996.tb00031.x>
- Kita S, Hasegawa A, Nakajima J, Okada T, Matsuzawa T, Katsumata K (2012) High-resolution seismic velocity structure beneath the Hokkaido corner, northern Japan: arc-arc collision and origins of the 1970 M 6.7 Hidaka and 1982 M 7.1 Urakawa-oki earthquakes. *J Geophys Res* 117:2301. <https://doi.org/10.1029/2012jb009356>
- Moriya T (1972) Aftershock activity of the Hidaka Mountains earthquake of January 21, 1970 [in Japanese with English figure captions]. *J Seismol Soc Jpn* 24:287–297. https://doi.org/10.4294/zisin1948.24.4_287
- Moriya T, Miyamachi H, Katoh S (1983) Spatial distribution and mechanism solutions for foreshocks, mainshock and aftershocks of the Urakawa-oki Earthquake of March 21, 1982 [in Japanese with English figure captions]. *Geophys Bull Hokkaido Univ* 42:191–213. <https://doi.org/10.14943/gbhu.42.191>
- Naito H, Yoshikawa S (1999) A program to assist crustal deformation analysis [in Japanese with English figure captions]. *J Seismol Soc Jpn* 52:101–103. https://doi.org/10.4294/zisin1948.52.1_101
- Nakahigashi K et al (2012) Seismic structure of the source region of the 2007 Chuetsu-oki earthquake revealed by offshore-onshore seismic survey: asperity zone of intraplate earthquake delimited by crustal inhomogeneity. *Tectonophysics* 562–563:34–47. <https://doi.org/10.1016/j.tecto.2012.06.052>
- NIED (2018a) Focal mechanisms automatically determined by the AQUA system. http://www.hinet.bosai.go.jp/AQUA/aqua_catalogue.php?y=2018&m=09&LANG=en. Accessed 29 Nov 2018
- NIED (2018b) Recent Large Earthquakes. Tsukuba <http://www.hinet.bosai.go.jp/backnumber/?LANG=en&y=2018&m=09>. Accessed 29 Nov 2018
- Okada T et al (2005) Aftershock distribution and 3D seismic velocity structure in and around the focal area of the 2004 mid Niigata prefecture earthquake obtained by applying double-difference tomography to dense temporary seismic network data. *Earth Planets Space* 57:435–440. <https://doi.org/10.1186/BF03351830>
- Okada T et al (2012) Hypocenter distribution and heterogeneous seismic velocity structure in and around the focal area of the 2008 Iwate-Miyagi Nairiku Earthquake, NE Japan—possible seismological evidence for a fluid driven compressional inversion earthquake. *Earth Planets Space* 64:717–728. <https://doi.org/10.5047/eps.2012.03.005>
- Omuralieva et al (2012) Lateral variation of the cutoff depth of shallow earthquakes beneath the Japan Islands and its implications for seismogenesis. *Tectonophysics* 518–521:93–105. <https://doi.org/10.1016/j.tecto.2011.11.013>
- Research Group for Active Faults in Japan (1991) Active faults in Japan: sheet maps and inventories. Univ of Tokyo Press, Tokyo
- Ross ZE, Kanamori H, Hauksson E, Aso N (2018) Dissipative intraplate faulting during the 2016 M_w 6.2 Tottori, Japan earthquake. *J Geophys Res Solid Earth* 123:1631–1642. <https://doi.org/10.1002/2017JB015077>
- Sakai S et al (2008) Highly resolved distribution of aftershocks of the 2007 Noto Hanto Earthquake by a dense seismic observation. *Earth Planets Space* 60:83–88. <https://doi.org/10.1186/BF03352765>
- Shibutani T et al (2005) High resolution 3-D velocity structure in the source region of the 2000 Western Tottori Earthquake in southwestern Honshu, Japan using very dense aftershock observations. *Earth Planets Space* 57:825–838. <https://doi.org/10.1186/BF03351861>
- Shiina T, Takahashi H, Okada T, Matsuzawa T (2018) Implications of seismic velocity structure at the junction of Kuril-northeastern Japan arcs on active shallow seismicity and deep low-frequency earthquakes. *J Geophys Res Solid Earth* 123:8732–8747. <https://doi.org/10.1029/2018JB015467>
- Shimizu H et al (2006) Aftershock seismicity and fault structure of the 2005 West Off Fukuoka Prefecture Earthquake (M_{JMA} 7.0) derived from urgent joint observations. *Earth Planets Space* 58:1599–1604. <https://doi.org/10.1186/BF03352668>
- Shito A et al (2017) Seismic velocity structure in the source region of the 2016 Kumamoto earthquake sequence, Japan. *Geophys Res Lett* 44:7766–7772. <https://doi.org/10.1002/2017GL074593>
- Sieh K et al (1993) Near-field investigations of the landers earthquake sequence, April to July 1992. *Science* 260(5105):171–176. <https://doi.org/10.1126/science.260.5105.171>
- Takahashi H et al (1999) Velocity field of around the Sea of Okhotsk and Sea of Japan regions determined from a new continuous GPS network data. *Geophys Res Lett* 26:2533–2536. <https://doi.org/10.1029/1999GL900565>
- USGS (2018) Earthquake Hazard Program. <https://earthquake.usgs.gov/earthquakes/eventpage/us2000h8ty/executive>. Accessed 29 Nov 2018
- Wessel P, Smith WHF (1991) Free software helps map and display data. *EOS Trans AGU* 72:445–446
- Yoshida et al (2007) 3D velocity structure model of the Ishikari and Yufutsu sedimentary basins. *Ann Rep Act Fault Paleoeearthquake Res* 7:1–29
- Zhang H, Thurber CH (2003) Double-difference tomography: the method and its application to the Hayward fault, California. *Bull Seism Soc Am* 93:1875–1889. <https://doi.org/10.1785/0120020190>

Publisher's Note

Springer Nature remains neutral with regard to jurisdictional claims in published maps and institutional affiliations.

Submit your manuscript to a SpringerOpen® journal and benefit from:

- Convenient online submission
- Rigorous peer review
- Open access: articles freely available online
- High visibility within the field
- Retaining the copyright to your article

Submit your next manuscript at ► [springeropen.com](https://www.springeropen.com)